Proceedings of the 21st ICSMGE, Vienna, Austria, 14 – 19 June 2026. Pistrol, Adam & Schweiger (eds.)
Published by: ÖGG, Austrian Society for Geomechanics, Salzburg, Austria, ISBN 978-3-9503898-4-5
https://doi.org/10.53243/ICSMGE2026-1448

Behavior of Stone Column Mitigation in Silt-Interlayered Liquefiable Deposits: Finite Element Analysis

Arpit Jain, Sayanti Banerjee, Shivank Shekhar
Department of Civil and Environmental Engineering, Indian Institute of Technology, Patna, Bihar, India, ajain01@iitp.ac.in

Abhijit Chakraborty
Geotechnical Engineering Group, CSIR- Central Road Research Institute, Delhi-Mathura Road, New Delhi

Sayanti Banerjee
Department of Civil and Environmental Engineering, Indian Institute of Technology, Patna, Bihar, India

Shivank Shekhar
Department of Civil and Environmental Engineering, Indian Institute of Technology, Patna, Bihar, India

ABSTRACT: The emerging research on soil-heterogeneity depicted the vulnerability caused by the ignorance of interlayers, bedding formations, and underlain soil patches in the sub-soil strata. Such soil formations are prevalent near offshore beaches or landfills. Therefore, it is quite essential to assess the response of reinforcements or mitigation elements towards layered soil deposits. In the present study, a seismic environment has been chosen based on shaking table tests where UBC-3D PLM material model was utilised for analysis using finite element-based software. The numerical model was first validated using the outcomes of shaking table testing. In the further stages, stone columns were utilized in reducing the liquefaction susceptibility. It has been assessed that the behavior of pore pressure movement around the interface of stone columns and layered soil junction is found to be completely different from that of the homogeneous soil deposits. Furthermore, the variations in the parameters of stone columns were adopted for the optimization, which can truly assist modern practices of seismic-hazard mitigations near liquefaction-prone sites.

KEYWORDS: Liquefaction, Finite Element Analysis, Silt-interlayer, UBC3D-PLM.

1 INTRODUCTION

Recent earthquakes in Turkey, Assam (India), and Indonesia demonstrated the liquefaction-induced sand boiling, devastating settlements, and enormous flow slides. In the last few years, the geotechnical earthquake engineers and researchers emphasized the criticality of soil heterogeneity and associated soil liquefaction occurrences. Experimentally, such simulation has been performed using shaking table testing and centrifuge to investigate liquefaction occurrences near the embankments, bridges, and dams (Florin and Ivanov, 1961; Fiegel and Kutter, 1994). Additionally, Liu and Qiao (1984) and Kokusho (2003) pointed out the modification in liquefaction failures due to the presence of silty pockets patterns beneath key geotechnical structures and further development of water film layers. The comparative analysis of shaking table experiments and FEM results on liquefaction-consolidation provided insights about failure mechanisms (Ye et al. 2007). Several research studies focused upon the investigation of liquefaction vulnerability using cyclic triaxial tests on heterogeneous specimens after varying the thickness and number of participating soil layers (Jain et al. 2022a, Jain et al. 2022b, Jain et al. 2023a, Jain et al. 2023b). Researchers performed key simulations of liquefaction-induced phenomena using effective constitutive models for shaking table tests. In such cases, Akiyoshi et al. (1996) assessed the seismic response of 2D soil structure under saturated states after providing dynamic loadings. In a study performed by Byrne et al. (2004), centrifuge tests were simulated through numerical analysis where larger confining stresses were considered to notice the densification pattern. The results of FEM and FDM were compared through two-phase field-type constitutive models to understand the repeated process of liquefaction-consolidation. In a research work performed by Ozener et al. (2009), the Towahata-Iai model performed well in the simulation of liquefaction occurrences in stratified profiles developed in shaking table facility. The researchers performed both the numerical and experimental simulation through dynamic modes. UBCSAND model was considered by Ecemis (2013) for the simulation of 1-g shaking table tests and associated liquefaction failures in correlation with the experimental results. The outcomes of large shaking table tests have been numerically simulated using FLAC software and an optimized constitutive model in a study performed by Ecemis (2021), which demonstrated the criticality of liquefaction damages. The behavior of reconsolidation settlements has been numerically simulated by Basu et al. (2022), where the researchers considered centrifuge and shaking table tests at free field state. In recent years, simulation of liquefaction and its mitigation using finite element framework has shown considerable development using advanced constitutive models like UBC3D-PLM (Chakraborty and Sawant 2022, 2024).

In most of the studies based on mitigation against liquefaction-induced damages, soil heterogeneity has been poorly understood. This caused either underestimation or overestimation in the failure assessment. Therefore, this research work presents a stone column-based mitigation approach for liquefaction-induced failures, utilizing the experimental outcomes of shaking table tests. Additionally, after suitable validations, numerical models were developed.

2 MATERIALS, APPARATUS AND METHOLOGY

In the present research study, suitable shaking table tests were performed on both the homogeneous and heterogeneous specimens prepared using sand raining technique (Jain et al. 2022a). The shaking table assembly is capable of providing 1-g horizontal shaking, as considered in previous research studies (Ozener et al. 2009). All of these were performed at a frequency of 4Hz to replicate the liquefaction occurrences. The materials used in the study were fine sand and silt. In order to capture the response of developed pore pressure, PPT (pore pressure

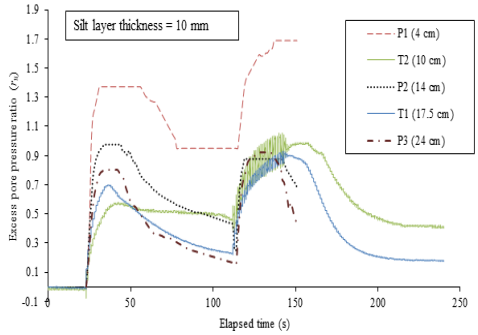

Figure 2. Pore pressure response of the stratified specimens with a silt thickness of 10 mm.

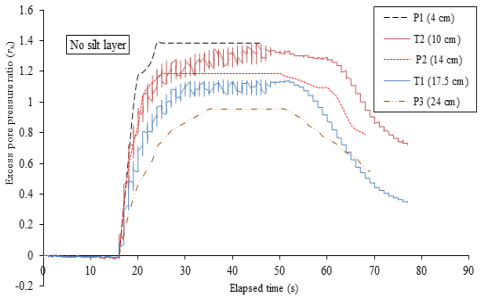

Figure 3. Excess pore pressure of the homogeneous sand specimen.

transducers) were used, which are capable of collecting 200 data points in a single second.

3 SPECIMEN TYPE AND CALCULATION APPROACH

The specimens considered were of two different categories, i.e. homogeneous and layered type. The specimen with layered features consists of a silt layer with a thickness of 10 mm. This silt layer is responsible for hindering pore pressure movement to modify the failure patterns of conventional liquefaction. To understand such features, the PPTs were located at different depths as shown in Figure 1.

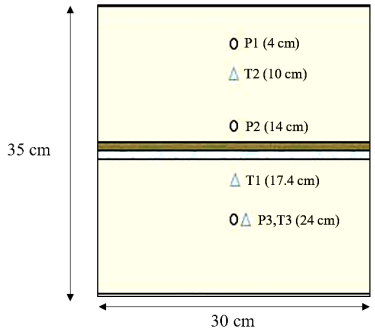

Figure 1. Location of different pore pressure transducers and piezometers used in the shaking table

The formulation of relative density in layered or heterogeneous specimens is quite different than that of homogeneous ones. Therefore, many researchers considered suitable equations for finding the overall relative density of the prepared specimens (Yoshimine and Koike, 2005, Xiu et al., 2019; Jain et al., 2022). In this research work, these equations (Eq. 1, Eq. 2, Eq. 3, Eq. 4) were also used to calculate the overall density of the specimens.

$$D_{r,m} = \frac{e_{\max,m} - e}{e_{\max,m} - e_{\min,m}} \quad \text{Eq. 1}$$

$$e_{\max,m} = \sum[R_{m,i}(e_{\max,i} + 1)] - 1 \quad \text{Eq. 2}$$

$$e_{\min,m} = \sum[R_{m,i}(e_{\min,i} + 1)] - 1 \quad \text{Eq. 3}$$

Where $D_{r,m}$ (modified relative density), $e_{\max,m}$ (modified maximum void ratio), $e_{\min,m}$ (modified minimum void ratio), e_e, (equivalent void ratio) and $R_{m,i}$ (percentage of the dry weight of i_{th} layer in the layered soil)

4 RESULTS AND DISCUSSION

In this research work, the onset of liquefaction is considered when, due to the increase in excess pore pressure, the effective stress diminishes and becomes zero. Such phenomenon has been investigated by See and Lee (1966) using a term called pore pressure ratio, which can be represented as:

$$r_u = \frac{\Delta u}{\sigma_c'} \quad \text{Eq. 4}$$

Where, σ'_c = effective confining stress and u = Pore pressure

All the specimens, found to be liquefied when pore pressure reaches unity. In the present research work, 1g shaking table experimental tests on homogeneous and layered soil specimens have been demonstrated. Additionally, the experimental outcomes have been numerically simulated and validated at a frequency of about 4 Hz. The stone column-based ground improvement technique has been performed on both the homogeneous and layered soil mass. The detailed investigations have been presented as follows.

4.1 *Experimental output from shaking table tests:*

In Figure 2 and Figure 3, the pore pressure response of layered and homogeneous sand specimens is presented. In the case of layered specimen first a seismic motion of single second was provided followed by post-liquefaction observation (Figure 2). Then, again, a post-seismic motion of 30 seconds was applied to understand the criticality caused by post-liquefaction occurrences. For the homogeneous specimens, a complete seismic motion of 30 seconds was provided (Figure 3). In Figure 2, It can be noticed that the highest pore pressure ratio found to be at 4 cm from the top of the specimens. Additionally, the lowest rate of pore pressure ratio found at 24 cm from the top. After the plateau of excess pore pressure ratio, the dissipation of pore pressure after the completion of dynamic motion found to be the highest at a depth of 4 cm from the top of the specimen. Different locations of pore pressure transducers provided the salient details of pore pressure movement.

4.2 *Finite Element Modeling and Validation*

The behaviour of silt interlayered liquefiable deposits is complex, and simulating this phenomenon needs attention in terms of material constitutive model selection, calibration, and validation of system response concerning laboratory experiments. In a recent study by Chakraborty and Sawant (2025), it has been reported that silt layer significantly alters the response of a liquefiable deposit. However, very few studies emphasized the behaviour of mitigation response of such layered deposit. In the present study, the silt-interlayered liquefiable deposit is first simulated using the PLAXIS 3D finite element program. The soil layers are modeled using the UBC3D-PLM constitutive model while considering calibration

of the model parameters. UBC3D-PLM developed by (Beaty and Byrne 1998), is an effective stress-based elastoplastic material model for sand, designed to simulate liquefaction behaviour under dynamic loadings. The model utilizes the Mohr-Coulomb yield criterion within a three-dimensional principal stress space. The mobilized friction angle [(Φ_{mob})60] and plastic shear strain defines the hardening rule, following the principles of the Duncan-Chang approach and classical plasticity theory. The model adopts a non-associative flow rule based on the Drucker-Prager plastic potential function. Petalas and Galavi (2013) proposed an empirical correlation linking the corrected SPT value [(N_1)60] with the parameters of the UBC3D-PLM model. The parameters K_B^e, K_G^e and K_G^p are stiffness coefficients that primarily govern the nonlinear stress-dependent behavior of stiffness through the use of power law exponents me, ne, and np. The failure ratio (R_f) is typically assumed to lie within the range of 0.5 to 1.0. Parameters $f_{ac,hard}$, and $f_{ac,post}$ control the densification characteristics and post-liquefaction response of saturated sand. To keep the paper concise, only a brief overview of the model is provided here; detailed descriptions are available in (Petalas and Galavi, 2013). In a study, Chakraborty and Sawant (2022) highlighted that the model parameter K_G^p is a key factor governing the occurrence of liquefaction. Based on the best-fit liquefaction strength curve from the study by Idriss and Boulanger (2008), this parameter has been considered for a particular state of sand.

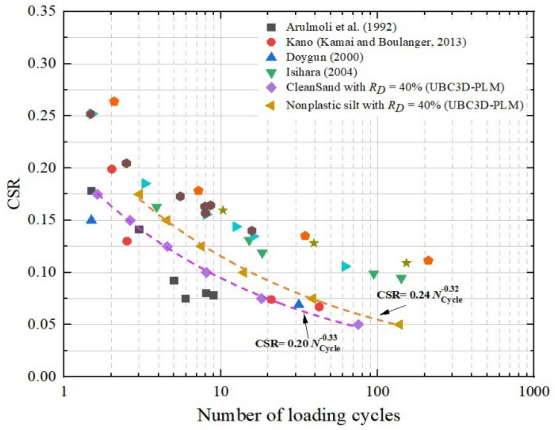

Figure 4. Calibration of sand and silt layers (R_D = 40%).

Figure 4 shows the calibration of model parameters considering liquefaction strength curve for both the sandy and silty soil for 40% R_D. It is clearly observed that silty soil has higher liquefaction resistance than the sandy soil. The corresponding calibrated model parameters are reported in Table 1. To validate the efficacy of the model in capturing the response of stratified liquefiable deposit, a finite element (FE) model is developed in PLAXIS. The sand and silt layers are considered to have a relative density = 40%. Initially, the homogenous and silt-interlayered deposits are scaled 10 times to the laboratory shake table geometry as discussed in section 4.1, and the non-dimensional r_u time histories are compared with the laboratory test results.

Table 1. UBC3D-PLM model parameters.

Parameters	Sand	Silt	Stone Column
K_B^e	566.6	656.2	744.2
K_G^e	809.4	937.4	1063
K_G^p	350	550	4466
m_e	0.5	0.5	0.5
n_e	0.5	0.5	0.5
n_p	0.4	0.4	0.4
R_f	0.83	0.83	0.64
$f_{ac,hard}$	0.45	0.45	0.65
$f_{ac,post}$	0.1	0.1	0.1
Permeability, k (m/s)	6.6×10^{-5}	7.4×10^{-6}	0.10

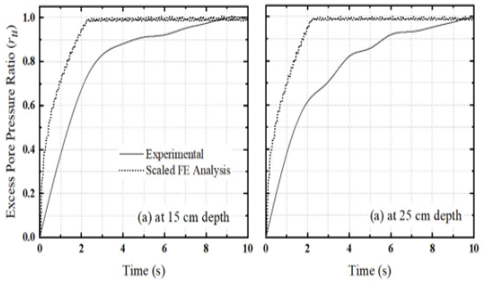

Figure 5. Comparison of r_u time history at two different depths with a 10 mm thick silt layer.

Figure 5 shows that FE model predicts early onset of initial liquefaction. However, as the time of loading progresses, a good match of r_u can be observed between the laboratory and FE results.

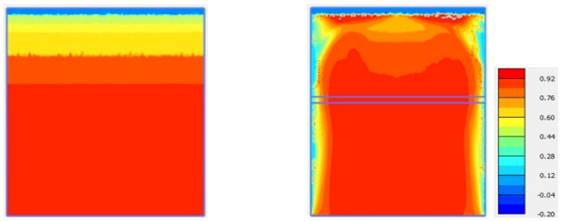

(a) Homogeneous deposit (b) Silt-interlayered deposit

Figure 6. r_u Contours plot for (a) homogeneous; (b) silt-interlayered liquefiable deposits.

4.3 Mitigation of Liquefaction using Stone Column:

Once the FE modeling is validated with the in-house shake table testing results, the mitigation approach considering the stone column is introduced in the FE models. Where the behaviour of a single stone column is evaluated in the case of silt-interlayered liquefiable deposit. A soil domain of 20 m × 20 m FE soil model developed. A silt interlayer at the middle of the sand layer is considered thickness of 0.10 m.

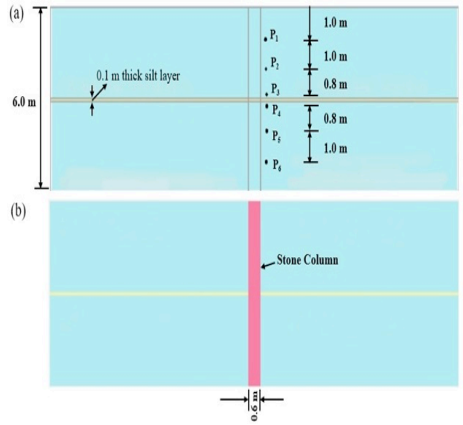

Figure 7. (a) Benchmark model without mitigation; (b) model with stone column mitigation.

The model without stone column mitigation is considered to be the benchmark model. Whereas in another model, a stone column is considered at the center of the soil domain. The stone column diameter is considered as 0.6 m, and the drainage boundaries are considered to be fully permeable. The detailed model parameters of the stone columns are reported in Table 1.

In the silt interlayered deposits, a visible change in the contours of pore pressure ratio can be visualized (Figure 6). Figure 7 shows the detailed configuration of the benchmark model and the model with stone column mitigation. Where the locations of predicted EPP response are highlighted (0.6 m distance from the center of stone column). Figure 8 shows the FE mesh models for both configurations. As an input loading, the acceleration time history of the 1989 Loma-Prieta earthquake is considered (Figure 9).

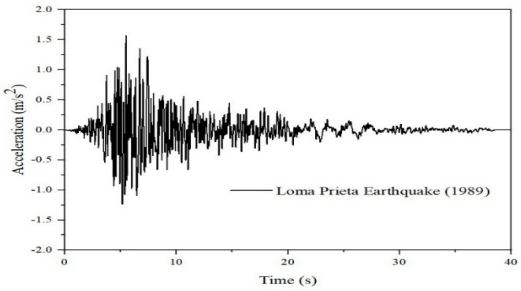

Figure 9. Acceleration time history used in this study.

The free-field boundary condition is considered for simulating the dynamic response of both models. Free-field boundary condition is efficient in absorbing incoming seismic waves, minimizing the reflection of waves from the model boundary, and simulating an infinite domain laterally. The acceleration input motion is given at the base of the FE models, considering a compliant base. A compliant base boundary effectively simulates the continuation of wave propagation into deeper soil layers while minimizing reflections at the bottom boundary. A fine mesh is adopted in the silt interlayer, and a medium mesh along with refinement around the silt interlayer is considered in the sand layers. The model parameters are considered based on Table 1. Whereas a rigid interface is considered between the stone column and the surrounding soil layers. Modeling the interface between stone columns and surrounding soil as rigid simplifies the numerical analysis by assuming perfect bonding and no relative displacement at the boundary.

Figure 10 shows the EPP time histories of P1 to P6 locations (as depicted in Figure 7). At shallow depth (P1) in case of the benchmark model, maximum EPP of 8.56 kPa has been observed. Which showed a marginal dissipation at the later stage of loading. Due to the presence of the stone column, a negligible reduction in EPP can be observed (1.8%). However, a rapid dissipation of EPP can be observed due to the presence of the stone column. Almost 39.5% more dissipation can be observed at P1 location due to the stone column. Similarly, at P2 location, 66.5% reduction in EPP can be observed at the end of loading. This observation shows that with an increase in depth, the stone columns' performance increases. The locations P3 and P4 are located very close to the silt interlayer. The primary intention is to monitor the EPP response due to the presence of the stone column in the silt interlayer. At P3 location, due to the presence of stone column, almost a 12% reduction in maximum EPP can be seen. Also, at the end of the loading, the stone column is found to be reducing 70% EPP concerning the benchmark model. Moreover, at P4 location (just below the silt interlayer), a reduction in stone column

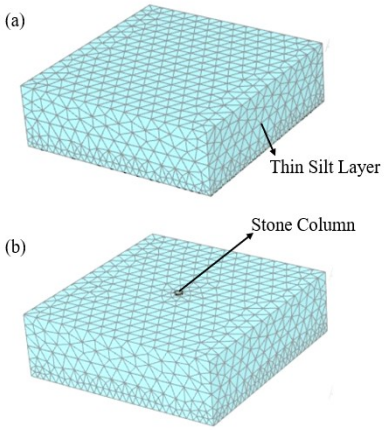

Figure 8. Finite element mesh of models (a) Benchmark; (b) Model with stone column.

performance is observed, which shows only 7% reduction in maximum EPP. Which indicates, the presence of silt interlayers hinders the efficacy of stone columns in reducing the effect of EPP.

However, at the end of loading marginal difference in dissipation of EPP is observed. At higher depths, the efficacy of stone columns in reducing maximum EPP response is reduced, which might be attributed to the presence of accumulated water due to the presence of silt interlayer. However, at the end of 100 s, the stone column is found to be reducing the EPP by 72.21% and 76% at P_5 and P_6 locations. This shows at greater depth that the stone columns are more effective in comparison to the shallow depth and the locations close to the silt interlayer.

Figure 11 shows the contour of r_u at the end of loading. This shows the critical role of silt interlayers in accumulating EPP as the permeability of the silt layer is lower than the sand layer, which hinders the migration of pore pressure. The stone column mitigation was found to reduce EPP, which was also found to be influenced by the presence of silt interlayers. However, the dissipation of excess pore pressure (EPP) is observed to be more effective in the sand layer above the silt interlayer, clearly highlighting the influence of the silt interlayer on post-liquefaction EPP dissipation.

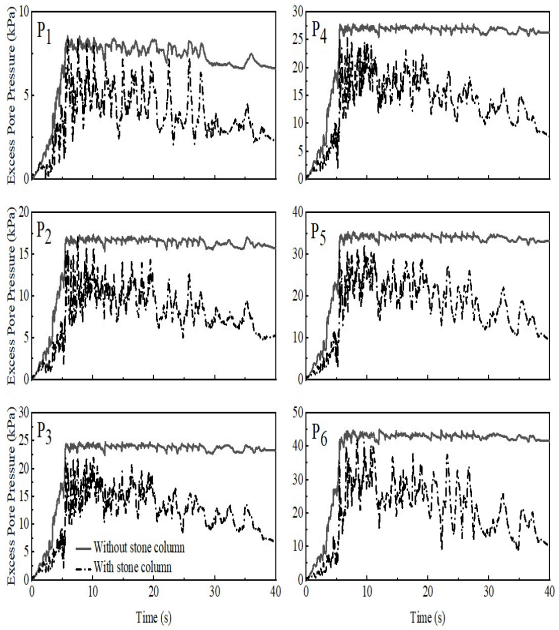

Figure 10. EPP time history at different locations for benchmark model and model with stone column.

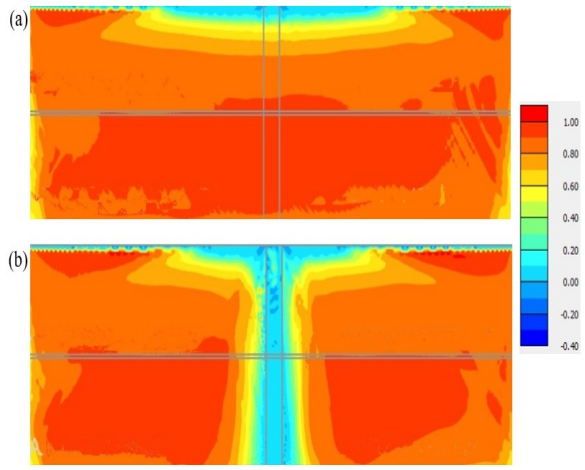

Figure 11. r_u contour of model(a) benchmark; (b) with stone column.

5 CONCLUSIONS:

The present research work focused upon the comparisons of shaking table testing and the FEM based analysis and mitigation of liquefaction occurrences in silt interlayered sandy deposits. There are few key outcomes obtained from the study, which are provided as follows:

1. From the laboratory shake table testing it has been found that the highest pore pressure ratio is found to be at 4 cm from the top surface of the soil. Additionally, the lowest rate of pore pressure ratio was found at 24 cm from the top.
2. FE model predicts early onset of initial liquefaction. However, as the time of loading progresses, a good match of r_u can be observed between the laboratory and FE results. The key aspects of liquefaction of silt interlayered deposit can be addressed using FEM based analysis.
3. The behaviour of a single stone column is evaluated in the case of silt-interlayered deposit, which suggests that stone column mitigation is effective in reducing the EPP surrounding the stone column within one diameter.
4. With an increase in depth, the efficacy of the stone column is found to be increasing. At shallow depth, the minimum reduction in maximum EPP can be observed.
5. The presence of silt interlayers significantly alters the EPP response around the stone column. However, in the dissipation stage, the stone column performance is marginally affected by the presence of the stone column.

6 REFERENCES

Akiyoshi, T., Fuchida, K., & Shirinashihama, S., 2001. Local site effects of transient dynamic characteristics of irregularly layered grounds.

Basu, D., Montgomery, J., & Stuedlein, A. W., 2022. Observations and challenges in simulating post-liquefaction settlements from centrifuge and shake table tests. Soil Dynamics and Earthquake Engineering, 153, 107089.

Beaty, M., and Byrne, P.M., 1998. An Effective Stress Model for Predicting Liquefaction Behavior of Sand. In: Geotechnical Earthquake Engineering and Soil Dynamics, pp. 766-777, Seattle, ASCE.

Byrne, P. M., Park, S. S., Beaty, M., Sharp, M., Gonzalez, L., & Abdoun, T., 2004. Numerical modeling of liquefaction and comparison with centrifuge tests. Canadian Geotechnical Journal, 41(2), 193-211.

Chakraborty, A., & Sawant, V. A., 2022. Numerical simulation of earthen embankment resting on liquefiable soil and remediation using stone columns. International Journal of Geomechanics, 22(11), 04022205.

Chakraborty, A., & Sawant, V. A., 2024. Response of embankment on liquefiable soil to sequential ground motions considering mitigation measures. Soil dynamics and earthquake engineering, 176, 108278.

Chakraborty, A., & Sawant, V. A., 2025. Dynamic Behaviour of Plastic and Non-plastic Silt Interlayered Liquefiable Deposit. Indian Geotechnical Journal, 1-22.

Ecemis, N., 2013. Simulation of seismic liquefaction: 1-g model testing system and shaking table tests. European journal of environmental and civil engineering, 17(10), 899-919.

Fiegel, G. L., & Kutter, B. L., 1994. Liquefaction mechanism for layered soils. Journal of geotechnical engineering, 120(4), 737-755.

Florin, V. A., 1961. Liquefaction of saturated sandy soils. In: 5th international conference on soil mechanics and foundation engineering, Vol. 1, pp. 107-111.

Idriss, I. M., & Boulanger, R. W., 2008. Soil liquefaction during earthquakes. Earthquake Engineering Research Institute.

Jain, A., Mittal, S., & Shukla, S. K., 2022. Cyclic behaviour of stratified soil under liquefied states. Marine Georesources & Geotechnology, 41(7), 721-742.

Jain, A., Mittal, S., & Shukla, S. K., 2022. Liquefaction proneness of stratified sand-silt layers based on cyclic triaxial tests. Journal of Rock Mechanics and Geotechnical Engineering, 15(7), 1826-1845.

Jain, A., Mittal, S., & Shukla, S. K., 2023. Energy-based approach to study liquefaction triggering in homogeneous and stratified soils under consolidated undrained cyclic loading. Engineering Geology, 321, 107151.

Jain, A., Mittal, S., & Shukla, S. K., 2023. Use of polyethylene terephthalate fibres for mitigating the liquefaction-induced failures. Geotextiles and Geomembranes, 51(1), 245-258.

Kokusho, T., 2003. Current state of research on flow failure considering void redistribution in liquefied deposits. Soil Dynamics and Earthquake Engineering, 23(7), 585-603.

Liu, H., & Qiao, T., 1984, July. Liquefaction potential of saturated sand deposits underlying foundation of structure. In: 8th World Conf. on Earthquake Engineering (Vol. 3, pp. 199-206).

Yoshimine, M., & Koike, R., 2005. Liquefaction of clean sand with stratified structure due to segregation of particle size. Soils and foundations, 45(4), 89-98.

Ecemis, N., 2021. Experimental and numerical modeling on the liquefaction potential and ground settlement of silt-interlayered stratified sands. Soil Dynamics and Earthquake Engineering, 144, 106691.

Tohumcu Özener, P., Özaydın, K., & Berilgen, M. M., 2009. Investigation of liquefaction and pore water pressure development in layered sands. Bulletin of Earthquake Engineering, 7(1), 199-219.

Petalas, A., & Galavi, V., 2013. Plaxis liquefaction model UBC3D-PLM. Plaxis report.

Xiu, Z., Wang, S., Ji, Y., Wang, F., & Ren, F., 2020. Experimental investigation on liquefaction and post-liquefaction deformation of stratified saturated sand under cyclic loading. Bulletin of Engineering Geology and the Environment, 79(5), 2313-2324.

Ye, B., Ye, G., Zhang, F., & Yashima, A., 2007. Experiment and numerical simulation of repeated liquefaction-consolidation of sand. Soils and Foundations, 47(3), 547-55.